Influence of nitrogen and temperature on the deposition of tetrahedrally bonded amorphous carbon

B. Kleinsorge,[a] A. C. Ferrari, J. Robertson, and W. I. Milne
Department of Engineering, University of Cambridge, Cambridge CB2 1PZ, United Kingdom

(Received 29 December 1999; accepted for publication 6 April 2000)

The effect of nitrogen addition on the properties of tetrahedral amorphous carbon (ta-C) has been studied. The ta-C is deposited by a filtered cathodic vacuum arc. The effect of introducing nitrogen on its plasma was measured by a retarding field analyzer and optical emission spectroscopy. The ta-C:N films were studied as a function of nitrogen content, ion energy, and deposition temperature. The incorporation of nitrogen was measured over the range of 10^{-2}–10 at. % by secondary ion mass spectrometry and elastic recoil detection analysis. The N content was found to vary slightly sublinearly with the N_2 partial pressure during deposition. A doping regime was found for N contents of up to 0.4 at. %, in which the conductivity changes while the sp^3 content and the optical band gap remain constant. For 0.4%–8% N, the sp^3 fraction remains above 80% but the optical gap closes due to a clustering of sp^2 sites. Only above about 10% N, the sp^3 fraction falls. The influence of nitrogen on the *a*-C was found to be independent of ion energies between 20 and 220 eV. Deposition above 200 °C causes a sudden loss of sp^3 bonding. Raman and optical gap data show however that existing sp^2 sites begin to cluster below this temperature. © *2000 American Institute of Physics.* [S0021-8979(00)00614-9]

I. INTRODUCTION

Amorphous carbon and amorphous carbon–nitrogen compounds have been of considerable interest in recent years. They have found applications as hard coatings on tools, bearings, optical instruments, and magnetic hard disks. Amorphous carbon deposited using highly ionized energetic ion beams such as filtered cathodic vacuum arc (FCVA), mass selected ion beam deposition, or pulsed laser deposition can have sp^3 bonded fractions of 80%–90%. This material is often referred to as tetrahedrally bonded amorphous carbon (ta-C),[1] or, in the hydrogenated form as hydrogenated tetrahedral amorphous carbon (ta-C:H).[2] These materials are semiconductors with band gaps over 2 eV.

The addition of nitrogen to amorphous carbon can have three effects. First, small additions of nitrogen can dope ta-C *n* type.[3–6] It was also found that about 0.1% N would improve the field emission properties of tetrahedral amorphous (ta-C).[7] Hence, nitrogen can change the electronic properties of ta-C.

Second, Liu and Cohen[8] have proposed that the compound C_3N_4 would show a hardness exceeding that of diamond. In this compound, carbon is entirely sp^3 bonded. This proposal led to considerable research on C–N compounds, but so far C_3N_4 has not been synthesized. It has proved difficult to achieve the high N incorporation and to maintain the C bonding as sp^3.[9–12] Except in double beam systems, high N contents require deposition at a higher N_2 pressure, which reduces the ionization of the plasma beam. A fundamental question arises whether the N content is limited by the deposition process or by the nature of C–N bonding in the solid. Similarly, is the reversion of C bonding to sp^2 at higher N_2 pressures due to the deposition process or to the nature of C–N bonding in the solid?

The third effect of nitrogen at pressures above 10^{-2} mbar in deposition systems is to create topological disorder in graphitic bonding. This leads to the formation of fullerene-like microstructures ('onions' or 'leaks') in films deposited by sputtering,[13,14] or by the cathodic arc,[15,16] generally at elevated temperatures. The films have a very high elastic recovery.

In this article we focus on relatively low concentrations of nitrogen and their influence on ta-C deposited with a FCVA. This extends our previous brief account of recently presented work[17] by linking film properties to the plasma properties. ta-C has very diamond-like properties: up to 85% sp^3 bonded carbon atoms, high hardness (up to 80 GPa), a resistivity of up to 10^8 $(\Omega\ \mathrm{cm})^{-1}$ and a band gap of 2–2.5 eV.[18–21]

Deposition at elevated temperatures leads to graphitization of the carbon films. Depositing ta-C at elevated temperatures leads to a change between mainly sp^3 like material to mainly sp^2 like material at transition temperatures which were found to vary between 150 °C[18] and 400 °C.[22] It is unclear why the deposition transition temperature varies so much between different deposition systems. Koskinen found that it depends on instantaneous deposition rate[22] while Chhowalla *et al.*[18] and Sattel *et al.*[23] found it was due to ion energies.

To investigate the influence of nitrogen on ta-C as well as the influence of deposition temperature on the ta-C structure we looked at structural, optical, and electric properties of nitrogenated amorphous carbon films deposited by a FCVA at various substrate temperatures.

[a]Author to whom correspondence should be addressed; electronic mail: byk20@eng.cam.ac.uk

II. EXPERIMENTAL DETAILS

The amorphous carbon films were deposited with a FCVA system described previously.[24] The arc current was kept constant at 75 A and the magnetic field induced by the coils was 20 mT. This provides a deposition rate of about 7 Å/s for pure ta-C. The base pressure of the system was 5×10^{-7} mbar or better. Nitrogen was introduced into the deposition chamber in the region of the filter bend. All nitrogen pressures given are before the arc runs. Samples were simultaneously deposited onto quartz and silicon substrates. Samples on quartz are for optical and conductivity measurements while samples on silicon are for ellipsometry, Raman, or other structural measurements. The substrates could be biased with either a dc voltage or, for insulating substrates, given a self-bias by applying a high frequency to the substrate holder. The incident ion energy is given by the sum of the bias voltage and the initial ion energy of the C plasma. The Si substrates were subjected to a HF clean before mounting. The substrate holder could be heated and the temperature was monitored with a thermocouple. The substrates were held at temperature for at least 1 h prior to deposition. During deposition the temperature usually rose about 10 K. A series of films was deposited at room temperature, 80 °C, 100 °C, 150 °C, 200 °C, 250 °C, and 300 °C at various nitrogen pressures. Another series of films was deposited at base pressure, 2×10^{-4} mbar nitrogen partial pressure and 10^{-3} mbar nitrogen partial pressure and at various temperatures. The thickness of all films was determined by single beam ellipsometry or a Dektak profilometer.

The nitrogen content of films with over 2% N was measured by elastic recoil detection analysis (ERDA). Secondary ion mass spectroscopy (SIMS) was used for samples with lower N contents. The SIMS data were calibrated by comparing the ratio of the CN^- ion signal to that of negative carbon ions for samples of known N content measured previously by ERDA. All nitrogen contents are given as the x in $C_{1-x}N_x$ in %.

The sp^3 fraction was determined by electron energy loss spectroscopy (EELS). For EELS, samples were deposited on Si substrates to a thickness of 20–30 nm, the Si etched away, and free-standing ta-C films mounted on copper grids. The measurements were performed in transmission with a purpose-built spectrometer with a primary energy of 170 keV.[25] The sp^3 content is derived from the carbon K edge by comparing the ratio of areas of the 285 eV peak and the 290 eV edge, as described by Berger *et al.*[26]

Raman measurements were performed on a Renishaw Raman microscope system 2000 and on a Jobin–Yvon T64000 spectrometer coupled with a notch filter, using a 514 nm Ar ion laser. The spectra in general show two features, a G peak at 1540–1600 cm^{-1} and a D peak around 1350 cm^{-1}. The spectra were fitted with a Breit–Wigner–Fano (BWF) function[27] for the G peak and a Lorentzian function for the D peak. The G peak position (G shift) is taken as the maximum of the BWF. The D peak was only fitted when it could be recognized in the spectra. The G peak is due to the relative stretching motion of sp^2 carbon atoms in rings or chains. The D peak is due to breathing modes of sp^2 rings.[28–30] The $I(D)/I(G)$ ratio was calculated as the ratio of the D and G peak heights.

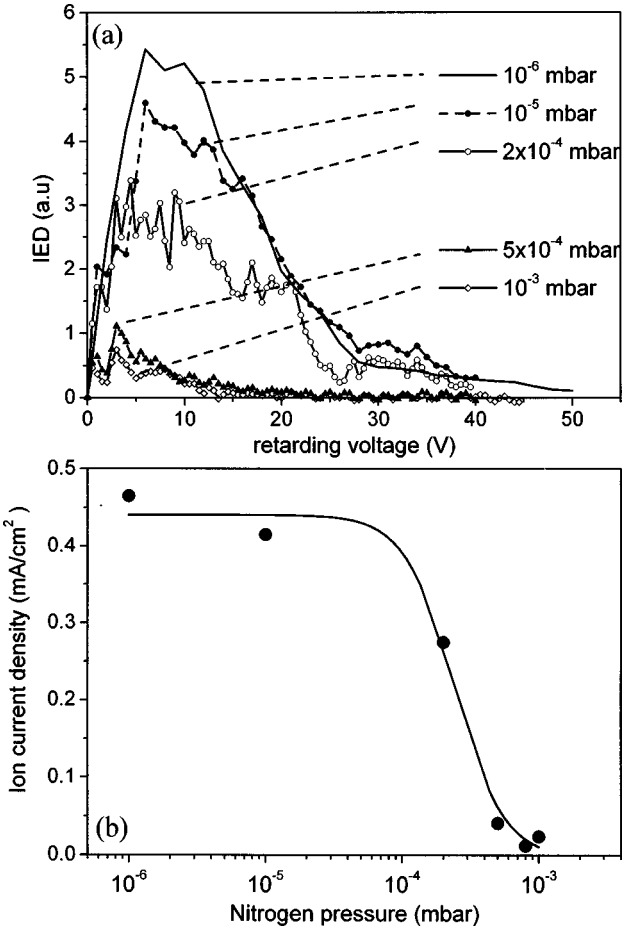

FIG. 1. (a) Ion energy distribution of plasma beam at different nitrogen pressures; (b) ion current density vs nitrogen pressure.

The optical band gap was determined from transmission and reflection spectra using an Ati-UNICAM UV-visible spectrometer. For conductivity measurements, Al electrode gap cells were evaporated on the films on quartz substrates and a Hewlett Packard 4140B pA meter was used for current–voltage measurements. The conductivity was measured over the temperature range from 300 to 470 K to derive the activation energy.

III. RESULTS

A. Plasma characterization

Properties of the deposition plasma were measured with a retarding field analyzer (Faraday cup) and optical emission spectroscopy (OES). Plasma characterization in cathodic arc systems is difficult due to excessive noise, which originates from the random movement of the arc spot on the cathode.[31] The spectra are an average of 20–30 measurements to reduce the noise.

Figure 1(a) shows the ion energy distributions measured at different N_2 pressures and Fig. 1(b) shows the ion current density. The ion energy distributions resemble a Maxwellian shape as they show a long tail. The intensity of the distributions changes strongly between 2×10^{-4} and 7

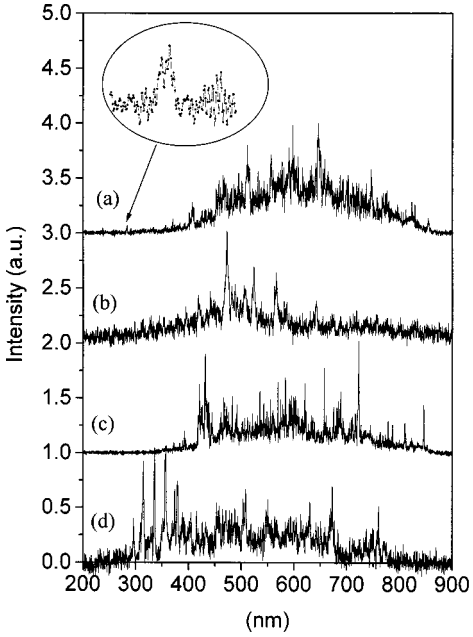

FIG. 2. Optical emission spectra of: (a) near cathode spot, no nitrogen, (b) sample position, no nitrogen, (c) 10^{-4} mbar nitrogen in cathode position, (d) 10^{-4} mbar nitrogen in sample position.

$\times 10^{-4}$ mbar. The ion current density remains constant up to 10^{-5} mbar and then decreases rapidly reaching 0.04 mA/cm^2 at 4×10^{-4} mbar. The peak of the ion energy distribution is at 7–8 eV, as seen previously.[32] The peak position falls as the ion current decreases above 10^{-4} mbar. Positive ion currents could be measured up to 30–40 V on the retarding cup. Above 10^{-4} mbar, ions could only be detected for up to 15–20 V on the retarding cup, which may, however, be due to very low currents and high noise.

The fraction of ions in the film forming particle flux was calculated from the ratio of ion current density and deposition rate, assuming only C^+ ions. The ion fraction was found to be 80% up to 10^{-4} mbar nitrogen, dropping to 10% at higher pressures. Note that this assumes only C^+ ions, no cluster ions, a sticking coefficient of 1 for ions, and a sputtering coefficient of 0.[33,34]

OES were taken in the cathode region and at the sample position. Figure 2 shows spectra taken at these two different positions at system base pressure and at 10^{-4} mbar nitrogen. For the arc running at base pressure, the OES has considerable background. This background is found in other carbon plasmas and has been attributed to a blackbody radiation from dust in the plasma.[35] In our case, the background is centered at 600 nm for cathode region spectra and at 500 nm for sample spectra. Few peaks can be attributed to atomic and molecular species with certainty, due to excessive noise. For cathode spectra, a peak at 283 nm is clearly seen and attributed to C^+, but the peak could not be seen at the sample position. The sample position spectra show a very strong peak at 470 nm due to the C_2 Swan bands ($A\ ^3\pi_g - X\ ^3\pi_u$)(660–440 nm). Other Swan band peaks are less pronounced. Swan band peaks were also found at the cathode, as well as peaks belonging to the Deslandres–D'Azambuja system ($c\ ^1\Pi_g - b\ ^1\Pi_u$ (340–400 nm) of C_2.

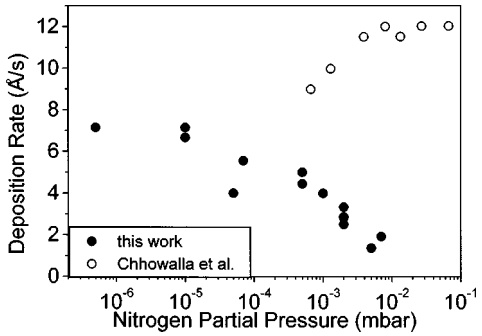

FIG. 3. Deposition rate of filtered cathodic vacuum arc and unfiltered cathodic vacuum arc (Chhowalla).

The background radiation clearly falls if nitrogen is introduced into the chamber. At 10^{-3} mbar N_2 at the sample position, it was no longer observed.

For 10^{-4} mbar N_2 pressure, the N_2 second positive system ($C\ ^3\Pi_u - B\ ^3\Pi_g$)(300–400 nm) and the N_2^+ first negative system ($B\ ^2\Sigma_u^+ - X\ ^2\Sigma_g^+$)(300–400 nm) dominated the spectrum at the sample position, while at the cathode position hardly any peaks came out of the noise in the 300–400 nm range. Peaks at 420 and 469 nm could however be attributed to the N_2^+ first negative system. At 10^{-3} mbar, the N_2^+ first negative system was also clearly visible in the cathode position with the N_2 second positive system. In the sample position at 10^{-3} mbar, the first positive system ($B\ ^3\Pi_g - A\ ^3\Sigma_u^+$)(550–750 nm) and the second positive system of neutral N_2 clearly dominate the spectrum.

B. Deposition rate

Figure 3 shows the deposition rates of samples deposited with the FCVA system. The figure also includes deposition rates found by Chhowalla *et al.*[36] using an unfiltered arc system. It is seen that the deposition rate for the filtered arc decreases with increasing nitrogen pressure, while the rate for the unfiltered arc increases with increasing p_{N_2}.

C. Nitrogen content of samples

Figure 4 shows the variation of nitrogen content of samples deposited at room temperature and at 100 eV ion energy as a function of the nitrogen partial pressure in the

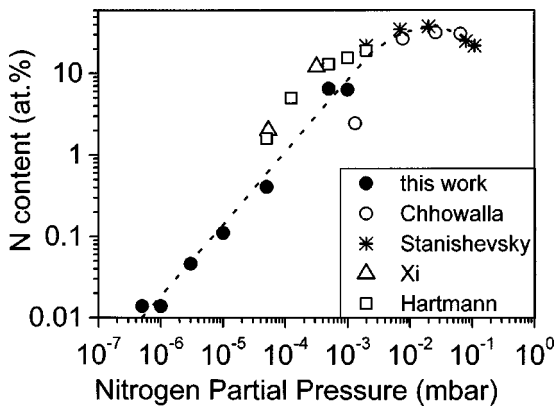

FIG. 4. Nitrogen content x in % (of $C_{1-x}N_x$) vs nitrogen partial pressure of this work and others.

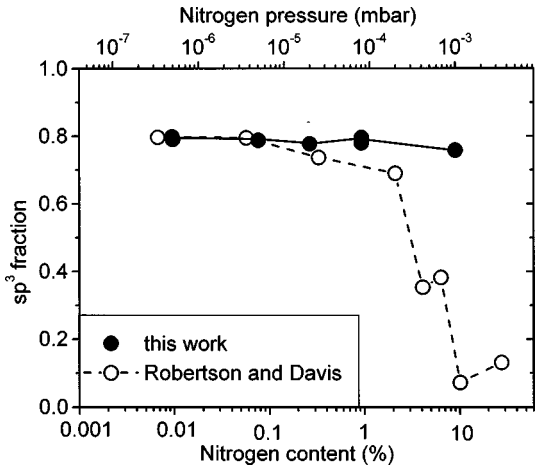

FIG. 5. sp^3 fraction vs nitrogen content for room temperature deposition. Data from Robertson and Davis are included for comparison (Ref. 5).

FCVA system. A fit to the data reveals that below a nitrogen pressure of 10^{-3} mbar the fraction of nitrogen atoms x_N (in at. %) varies as a slightly sublinear function of p_{N_2} (in mbar),

$$x_N \approx 4500^*(p_{N_2})^{0.9}.$$

Thus the films deposited at room temperature have a nitrogen content ranging from 0.01% to 8%. Figure 4 includes the data of Chhowalla,[36] Stanishevsky,[37] Hartman *et al.*,[38] and Shi[38] for comparison. The films of Chhowalla,[36] which have the lowest nitrogen incorporation for a given pressure, were deposited using an unfiltered arc, while Stanishevsky and Shi used deposition systems similar to our work. As the nitrogen pressure rises above 0.01 mbar, the nitrogen content saturates or even decreases. This limits the maximum N content of films produced by a single beam FCVA.

We observed a decrease of N content for deposition pressures above 10^{-3} mbar. A sample deposited at 7×10^{-3} mbar showed no nitrogen *K* edge in EELS.[39] ERDA was used to determine the N content of samples deposited at 10^{-3} mbar N_2 and floating potential at 100, 200, and 350 °C. The N content decreases linearly with deposition temperature: the x_N of the samples was 7%, 6%, and 4.5%, respectively. These results also show that the nitrogen incorporation is similar for 20 eV ion energy and 100 eV ion energy.

D. Room temperature deposition: Variation with nitrogen content

Figure 5 shows the variation of carbon sp^3 content deposited at room temperature and 100 eV ion energy as a function of N content. The sp^3 fraction remains at about 80% up to a N content of 9%. An extensive study of the carbon and nitrogen *K* edge of the films has been published recently by Waidman *et al.*[39] Davis *et al.*[3] found that FCVA films at higher N contents become sp^2 bonded.

Visible Raman spectroscopy was used to probe the configuration of the sp^2 sites. For room temperature deposition, the spectra were fitted with a BWF function for the *G* peak only. Even though a small *D* peak could be fitted for N contents between 1 and 10 at. %, fitting only one *G* peak to all the spectra gave more consistent results. Figure 6(a) shows the position of the *G* peak as a function of N content for samples deposited at 100 eV. The *G* peak remains at 1570 cm^{-1}, as in pure ta-C, up to $\sim10^{-5}$ mbar (0.2%N), and then decreases up to 10^{-3} mbar N_2 (9%N), after which it increases again. Figure 6(b) shows the *G* peak full width half maximum (ΔG). ΔG shows the opposite trend to the *G* position; it increases with increasing N_2 pressure up to 10^{-3} mbar (9% nitrogen). Thereafter it decreases again.

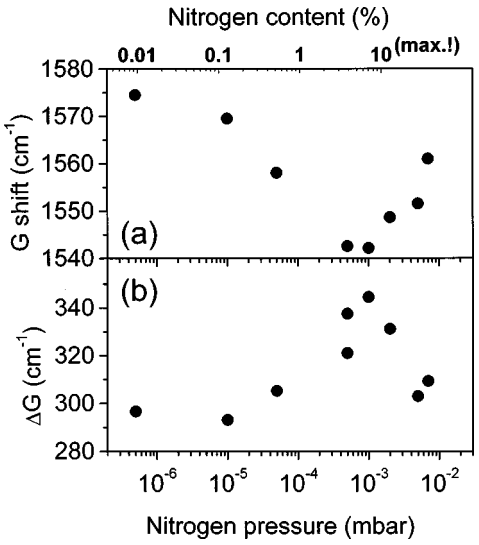

FIG. 6. (a) Raman *G* shift and (b) *G* full width half maximum vs nitrogen pressure for room temperature deposition. The upper axis (nitrogen content) is only valid to 10% nitrogen. For higher pressures we found a decrease in nitrogen content.

Figure 7(a) shows the optical band gap (Tauc) determined by transmission–reflection measurements, as a function of N content. The gap remains above about 2.0 eV until an N content of 0.4% (2×10^{-5} mbar), and then it decreases gradually with further N addition. This decrease in the gap is consistent with the detection of a *D* peak. Note that this decrease occurs while the sp^3 content is constant.

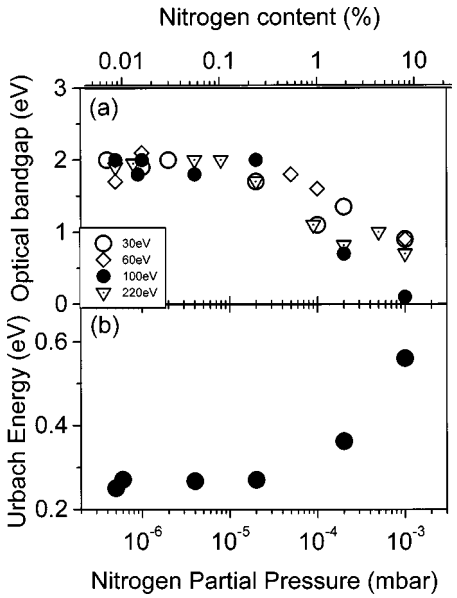

FIG. 7. (a) Optical gap for samples deposited at different ion energies; (b) Urbach energy of samples deposited at 100 eV vs nitrogen pressure.

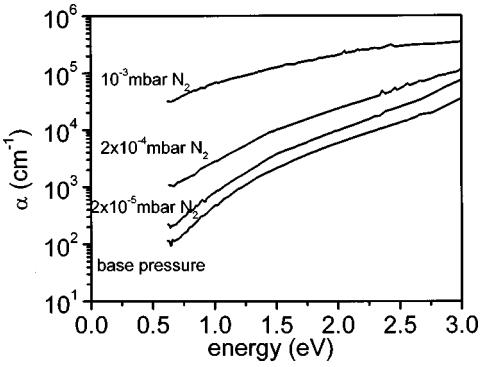

FIG. 8. Absorption coefficient α vs photon energy.

Photothermal deflection spectroscopy measurements were performed to determine the optical absorption edge. Figure 8 shows optical absorption coefficient as a function of photon energy. The absorption edge has a roughly exponential region, from which the Urbach energy E_u can be defined

$$\alpha(h\nu)=\alpha_0 \exp(h\nu/E_0),$$

where $\alpha(h\nu)$ is the absorption coefficient as a function of photon energy. E_u is a measure for the width of the wider band tail.[40] The absorption coefficient varies steadily with photon energy, without the clear distinction between band and tail regions seen in a-Si:H, so E_u is determined at $h\nu = 1$ eV. Figure 7(b) shows E_u as a function of N content, where a sudden increase occurs for N contents over 1% (10^{-4} mbar), indicating a broadening of the band tails.

Figures 9(a) and 9(b) show the room temperature conductivity and conductivity activation energy, respectively. Samples were deposited at four different substrate biases resulting in different ion energies. In this case the influence of the ion energies is marginal compared to the influence of nitrogen. Samples deposited at room temperature with no nitrogen show a room temperature conductivity of $10^{-6}\,(\Omega\,\mathrm{cm})^{-1}$. The conductivity increases slowly with N content to $10^{-4}\,(\Omega\,\mathrm{cm})^{-1}$ at 1% N, and it then increases more rapidly to reach about 1 $(\Omega\,\mathrm{cm})^{-1}$ at 9% N. In all cases the conductivity increases exponentially with T. A slight increase in activation energy of about 0.02–0.04 eV was observed between room temperature and 450 K (see Fig. 10). Figure 9(b) shows that, for all but one series, a slight maximum in the activation energy at p_{N_2} of 10^{-6} mbar could be observed. In two sets of samples, a slight increase in optical gap is also seen at this p_{N_2}. The exponential prefactor σ_0 lies between 0.1 and 1 $(\Omega\,\mathrm{cm})^{-1}$ and did not show a dependence on nitrogen pressure.

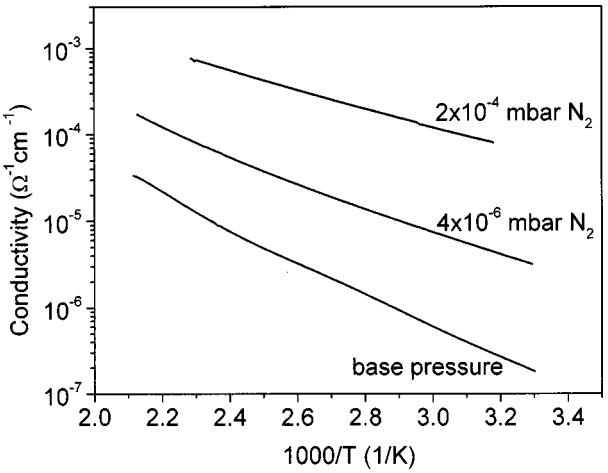

FIG. 10. Arrhenius plot for samples deposited at 100 eV ion energy.

E. Depositions at elevated temperatures

Figure 11 shows the variation of the Raman G shift and $I(D)/I(G)$ ratio with deposition temperature, for films de-

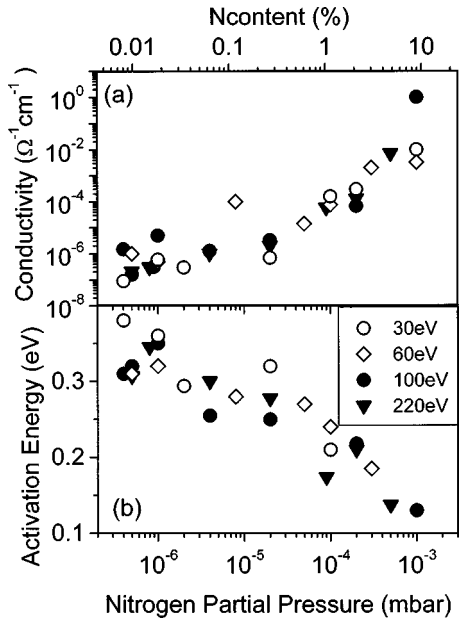

FIG. 9. (a) Conductivity and (b) conductivity activation energy for films deposited at different ion energies vs nitrogen pressure.

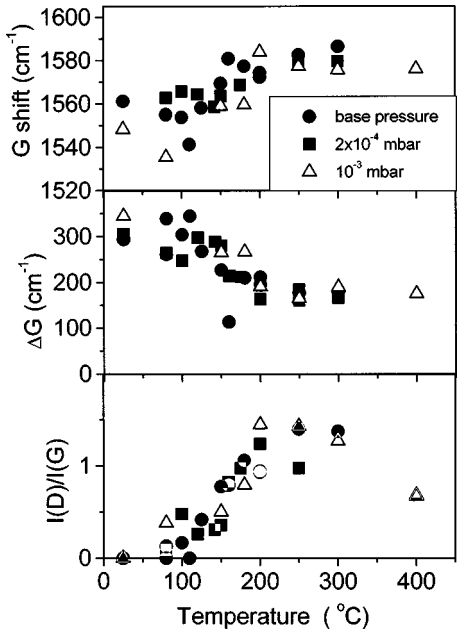

FIG. 11. Raman G shift, ΔG, and $I(D)/I(G)$ of samples deposited at various nitrogen pressures vs deposition temperature.

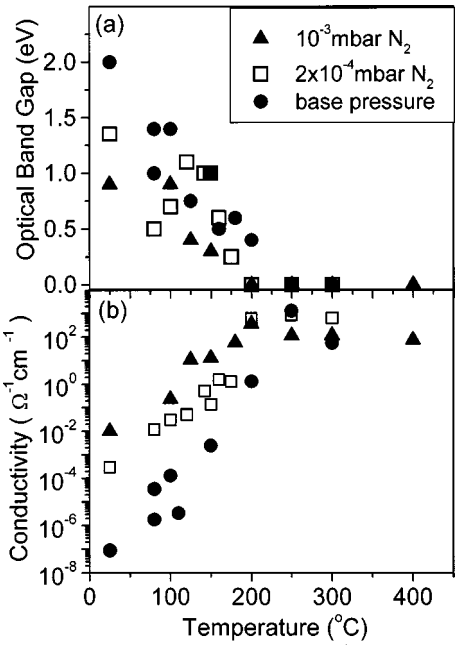

FIG. 12. Conductivity and band gap vs deposition temperature.

posited at base pressure, 2×10^{-4} mbar, and 10^{-3} mbar nitrogen pressure (all films deposited at floating potential). For all values, the nitrogen pressure during deposition had little influence. Despite the scatter, there is an increase in *G* peak for all three pressure series up to a deposition temperature of 200 °C, after which the value saturates. A *D* peak only starts to appear above 100 °C. At this temperature, ΔG decreases until it levels off at ~200 °C, just like the $I(D)/I(G)$ and the *G* position.

Figures 12(a) and 12(b) show the optical band gap (Tauc) and the conductivity versus deposition temperature, respectively, for the three nitrogen deposition pressures. The optical gap is decreasing steadily with increasing deposition temperature, and samples with higher N content show a smaller gap. Samples deposited at room temperature clearly show a higher gap than samples deposited at 80 °C. Samples above deposition temperatures of 200 °C did not show an optical gap any more.

The conductivity increases exponentially between room temperature and 200 °C from 10^{-7} to 10 $(\Omega\,\mathrm{cm})^{-1}$ and shows a strong dependency on N content. Above 200 °C the conductivity becomes almost independent of N content and its dependence on temperature declines.

Figure 13 shows the conductivity as a function of nitrogen partial pressure for samples deposited at constant temperatures. The influence of nitrogen on the conductivity of the samples decreases with increasing temperature. While at room temperature nitrogen increases the conductivity 5 orders of magnitude, at 150 °C the increase due to nitrogen is still 4 orders of magnitude while at 300 °C it is only 1 order of magnitude.

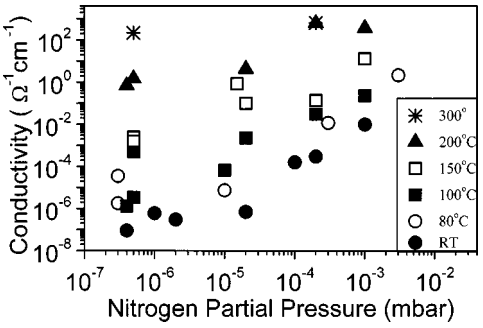

FIG. 13. Conductivity of samples deposited at various deposition temperatures vs nitrogen pressure.

IV. DISCUSSION

A. Deposition processes

Plasma characterization found that the ion current density reduces with nitrogen partial pressure. There is a large change between 2×10^{-4} and 5×10^{-4} mbar N_2 pressure. Bilek *et al.*[32,41] previously observed a shift towards lower ion energies due to the introduction of nitrogen into the FCVA. It was also observed that the ion energy distributions behind the filter bend followed the shape of a Maxwellian better than the shape of a Gaussian, which had been, measured previously.[18] In contrast to measurements by Bilek *et al.*[41] on a titanium arc in nitrogen atmosphere, a sharpening of the ion energy distribution with N_2 pressure was not seen, which might be due to charging effects of the analyzer at low ion energies.

OES showed colder background radiation (peaked at 600 nm) at the cathode region than at the sample region (peaked at 500 nm). This may be an effect of dust particle size. At the cathode region the moving cathode spot creates little explosions on the cathode surface, emitting dust particles up to the size of millimeters. These particles are expected to be colder than clusters or micrometer-size dust particles. We assume the background radiation at the cathode position is due to glowing big particles, while the background radiation at the sample position is due to clusters and micrometresize particles which still get through the filter, due to drag from the pump or reflection from the filter walls.

The spectra show the presence of Swan bands at 470 nm in the sample position and, weaker, at the cathode position. The weak Swan bands at the cathode position may be due to the excessive noise of macroparticles, rather than of a smaller fraction of C_2 in the plasma. C_2 is readily observed in laser ablation of carbon in the presence of background gases[42,43] and is believed to play a role in the formation of C_{60} molecules. In the FCVA, the clear presence of C_2 is a sign of the presence of neutrals after the filter bend. We believe that C_2 molecules travel around the bend due to the pressure gradient between the cathode region and the region of the sample holder (the FCVA is pumped by a large diffusion pump located beneath the sample holder and a smaller diffusion pump located near the cathode). We also found evidence for C^+ ions only in the cathode region. This may be due to low plasma throughput through the filter bend.

When nitrogen was introduced into the bend at 10^{-4} mbar at the cathode position only lines of the first negative system of N_2^+ (i.e., no evidence of neutral N_2 molecules) were observed, which means that the arc is able to ionize a large fraction of the nitrogen near the cathode. Only at a

pressure of 10^{-3} mbar nitrogen could some lines of the first negative system of the neutral N_2 molecule be detected at the cathode region. The spectra taken at the cathode position look different from spectra taken at the sample position. At the sample position at 10^{-4} mbar N_2, lines of the second positive system and the second negative system dominate the spectrum, and at 10^{-3} mbar the spectra is made up of the first and second positive system of neutral N_2. There might be some lines correlated to the first negative system, but neutral nitrogen is dominant. These results indicate that recombination of positive ions with electrons occurs on the way from the cathode to the sample position.

The deposition rate decreases with N pressure, but more slowly than the ion current density. This means that at higher N_2 pressures, neutrals must play an increasing role in the formation of ta-C:N films.

Figure 4 shows that N incorporation into the film is nearly linear with N_2 partial pressure at low p_{N_2} before saturation and even decreasing. N can enter the film by (a) being in the form N^+ or N_2^+, CN^+, (or other positive CN compound ions), being accelerated onto the film and penetrating the growing film by subsurface implantation (subplantation) or (b) by being physisorbed at the surface and then, by a knock-on process, being subplantated into the film, or (c) by being chemisorbed at the film surface and hence bonded to the growing film matrix. We found that the nitrogen incorporation into *a*-C films decreases at higher deposition temperature, as also observed by other groups.[14,44,45] Recently it was also found that the nitrogen etch rate of ta-C decreases with increasing temperature.[46] This was explained by physisorbtion of N_2 at the growing film surface and then ion impingement would release CN and N into the gas phase. The temperature dependence of the etch rate can be explained by the fact that adsorption is a process which increases with the square root of temperature while desorption increases exponentially with temperature, i.e., with increasing temperarure less nitrogen is adsorbed at the film surface and hence the etch rate decreases. We can assume a similar model for N incorporation during film growth, i.e., process (b) would be favorable to explain the film growth. The adsorption of N_2 on the film surface and the incorporation and binding to the growing film due to ion bombardment is also the favored model for TiN film growth.[47] It is in accordance with a linear increase of nitrogen in the films with nitrogen pressure.

Then why does the nitrogen content saturate at 30% and even decrease at higher pressures? This might be due to the deceleration of ions or other high energetic species, which are responsible for the knock-on process. Hence at higher N_2 pressures the ion energy is no longer sufficient to enhance the formation of CN bonds. The change in plasma properties could thus explain the decrease in N content at higher pressures. The only way to overcome the limit of nitrogen incorporation is to use an extra plasma source to ionize the nitrogen.[11] The different behavior of deposition rate with the filtered and unfiltered arc can be explained by graphitization due to nitrogen: In the pressure range where the deposition rate increases in the unfiltered arc, the nitrogen content exceeds 10%–15% and one can assume graphitization takes place. The same incoming flux of particles would then grow a film with lower density, which would increase the growth rate by a third, as observed.

B. Nitrogen and the sp^2 transition

Despite the high nitrogen pressures we have failed to deposit films with a N content over 9% and hence we could not observe a sudden transition to mainly sp^2 bonded material. On the contrary, deposition at pressures exceeding 10^{-3} mbar N_2 lead again to the formation of high sp^3 films. For 0.01%–10% N, the sp^3 fraction decreased by only 5%.

The fact that the sp^3 content stays nearly constant at N_2 pressures where the ionization is decreasing, i.e., between 10^{-4} and 10^{-3} mbar, suggests that the sp^2 transition above 10% is a bonding effect, not a plasma effect. A similar conclusion was reached by Hu *et al.*[12]

We could show that with increasing nitrogen content in the film the G peak shifted from 1570 to 1540 cm^{-1} while ΔG increased from 300 to 350 cm^{-1}. The decrease of the G shift indicates an increase in sp^2 bond length and the increase in ΔG indicates a larger variety of sp^2 bond lengths with increasing N content. The absence of a big D peak indicates that no appreciable sp^2 clustering into ordered rings takes place.[27–30] It should be noted that largest change in G shift and ΔG appears at pressures between 10^{-4} and 10^{-3} mbar, i.e., when the ion current density also changes drastically. Hence the observed change could not only be due to nitrogen, but also to a change in deposition process.

Note the optical gap decreases between 0.4 and 9 at. % N, while the sp^3 fraction remains constant. This implies that existing sp^2 sites are beginning to cluster and reduce the gap (and indeed a small D peak can be seen at higher nitrogen contents). A similar effect is observed for depositions of ta-C at higher T, and for annealing of ta-C to high T.[48,49] This is a key observation, as it means that conducting ta-C:N can be achieved simultaneously with high sp^3 content.

C. Doping of ta-C

At low N content and low deposition temperatures, the sp^3 fraction is high and constant and the optical gap 2 eV. In this regime, heterostructures on silicon suggest that nitrogen acts as a substitutional dopant of ta-C.[50] It was found previously that activation energy passes through a maximum at low N contents before decreasing again.[51,5] This behavior was attributed to the movement of the Fermi level from the lower part of the band gap through midgap to closer to the conduction band. Further evidence of this is that thin film transistors show that ta-C has *p*-type conduction[52] and that scanning tunneling spectroscopy also suggests a movement of the Fermi level with N addition.[53]

The present work does not find the previous strong maximum in activation energy corresponding to E_F passing through midgap. However, the value for the activation energy was measured at room temperature rather than at 500 K as reported previously.[5] Nevertheless, a weak maximum in activation energy and gap is seen for some samples at $p_{N_2} = 10^{-6}$ mbar. The conductivity prefactor σ_0 remains approximately constant in the measured regime from 0.01% to

9% N, even though the activation energy is changing. This contrasts with *a*-Si:H, where the prefactor changes by orders of magnitude when doping occurs. It should be pointed out that the doping effect in ta-C is weak, and conduction remains well within localized states. The density of localized states is so high that conduction is always by hopping within band tails, which is why σ_0 remains low.

D. Deposition at elevated temperatures

It was found before that ta-C changes rapidly from sp^3 rich to sp^2 rich at a certain transition deposition temperature. Chhowalla *et al.*[18] and Sattel *et al.*[23] found that the transition temperature decreases with increasing ion energy. Koskinen *et al.* using a pulsed arc even reported the deposition of sp^3 rich ta-C to temperatures up to 400 °C,[22] and found that the transition temperature increases with deposition rate. Figure 11 shows that a *D* peak starts appearing at a substrate temperature of about 80 °C, and saturation of *G* shift, ΔG and $I(D)/I(G)$ takes place at about 200 °C. This does not mean that the sp^2 to sp^3 transition starts at such low temperature. In fact, during high temperature deposition the clustering of the sp^2 phase happens before a significant conversion of sp^3 to sp^2 sites, as recently found.[49] A similar behavior is found for postdeposition annealed ta-C samples, where the *D* peak starts appearing before a transition to sp^2 bonded material takes place.[48] Given the similar deposition rate and sp^3 fraction of the as deposited samples in this work and in Ref. 18, we can assume that the transition temperature for the material deposited in this work is around 200 °C.[18]

E. Deposition at elevated temperatures with nitrogen

While Raman and the optical band gap did not give a clear trend between samples deposited at different nitrogen pressures at elevated temperatures, we could show that electronic properties of our samples deposited below 200 °C are influenced by nitrogen, while for samples deposited above this temperature nitrogen had decreasing influence. This was also shown by Hellgren *et al.*,[14] who showed that at low nitrogen concentrations (below 10%) and above 200 °C deposition temperature amorphous carbon is graphitelike.

We saw that nitrogen incorporation at room temperature leads to a broader *G* peak and decrease in the *G* shift, while deposition at elevated temperatures leads to an increase in *G* shift and a decrease in ΔG. An interpretation of this behavior is that, at room temperature, nitrogen leads to interlinking of sp^2 sites by chains, with no significative clustering of the sp^2 phase in rings. This is reflected in an increase of bond length and a broad distribution of oscillation modes. Deposition at elevated temperatures leads to ring structures (breathing modes), and higher frequencies. In fact, the films deposited at base pressure show an initial decrease in *G* shift for temperatures up to 100 °C after which the *G* shift value increases again. This is thought to be due to an intermediate stage, where sp^2 sites in chains lengthen before forming rings.

V. CONCLUSIONS

In our work we described the influence of nitrogen on plasma and film properties of a FCVA. It was found that the ion current density decreases sharply between 2×10^{-4} and 6×10^{-4} mbar N_2. Optical emission spectra revealed the presence of C_2 in the sample position even without any nitrogen present in the system. Nitrogen at 10^{-4} mbar was fully ionized at the cathode region, but neutral N_2 could be observed at the sample position. At 10^{-3} mbar neutral nitrogen could also be observed at the cathode position and no N_2^+ could be observed in the sample position.

The N content in our films reached a maximum of 9% and was nearly proportional to the pressure. Other authors reported with this or a similar method nitrogen contents of not more than 30%. At room temperature the sp^3 content of the samples remains high (80%) for up to 9% nitrogen in the samples. Higher nitrogen pressures lead to a decrease in nitrogen content in the films. The influence of nitrogen can be seen in Raman spectra, where a decrease in *G* shift and an increase in *G* width is observed, which is attributed to the formation of sp^2 chains. Deposition at increased substrate temperatures leads to an increase in *G* shift and a decrease in ΔG, which is attributed to the formation of graphitic ring structures. For room temperature deposition the gap started closing at 0.4 at. % (2×10^{-5} mbar) nitrogen in the films; at the same value the Urbach energy starts increasing. The conductivity starts increasing at smaller amounts of nitrogen, but shows a sharp increase at this value. Changes in the ion current density at 10^{-4} mbar nitrogen seem to be uncorrelated to these changes in the film. A slight maximum in activation energy at about 0.01% nitrogen can be observed, attributed to a slight doping effect of nitrogen. For films deposited at increased substrate temperatures a closing of the gap is observed for depositions at 80 °C and the gap is fully closed at 200 °C. Conductivity and band gap are dependent on nitrogen and temperature, but for increasing temperature nitrogen becomes less influential. The transition temperature of ta-C:(N) from mainly sp^3 bonded to a mainly sp^2 bonded material was found to be independent on nitrogen pressure and could be estimated to be 200 °C.

ACKNOWLEDGMENTS

The authors thank Dr. M. Siegal from Sandia National Laboratories, and Dr. H. Busch, University of Bonn, Germany, and Dr. W. Fukarek and Dr. U. Kreissig, FZ Rossendorf, Germany, for ERDA measurements. They also want to thank S. Hearne of the NMRC in Cork, Ireland, for SIMS measurements and M. Mooney, NMRC, Ireland, and C. E. Bottani, Politecnico of Milano, Italy, for Raman facilities. The authors are particularly grateful to Stephan Waidmann, Dresden, for EELS analysis. The authors also acknowledge EPSRC funding, LSF funding from the European Union for measurements at NMRC Cork. B. K. and A. C. F. are Marie Curie Fellows funded by the EU.

[1] D. R. McKenzie, Rep. Prog. Phys. **59**, 1611 (1996).
[2] M. Weiler, S. Sattel, K. Jung, H. Ehrhardt, V. S. Veerasamy, and J. Robertson, Appl. Phys. Lett. **64**, 2797 (1994).
[3] C. A. Davis, D. R. McKenzie, Y. Yin, E. Kravtchinskaia, G. A. J. Ama-

ratunga, and V. S. Veerasamy, Philos. Mag. B **69**, 1133 (1994).
[4] V. S. Veerasamy, J. Yuan, G. A. J. Amaratunga, K. W. R. Gilkes, M. Weiler, and L. M. Brown, Phys. Rev. B **48**, 17954 (1993).
[5] J. Robertson and C. A. Davis, Diamond Relat. Mater. **4**, 441 (1995).
[6] N. M. J. C. Conway, W. I. Milne, and J. Robertson, Diamond Relat. Mater. **7**, 477 (1998).
[7] B. S. Satyanarayana, A. Hart, W. I. Milne, and J. Robertson, Diamond Relat. Mater. **7**, 656 (1998).
[8] A. Liu and M. Cohen, Science **245**, 841 (1989).
[9] D. Marton, K. J. Boyd, A. H. Al-Bayati, S. S. Todorov, and J. W. Rabalais, Phys. Rev. Lett. **73**, 118 (1994).
[10] K. J. Boyd, D. Marton, S. S. Todorov, A. H. Al-Bayati, J. Kulik, R. A. Zuhr, and J. W. Rabalais, J. Vac. Sci. Technol. A **13**, 2110 (1995).
[11] S. E. Rodil, W. I. Milne, J. Robertson, and L. M. Brown (unpublished).
[12] J. Hu, P. Yang, and C. M. Lieber, Phys. Rev. B **57**, R3185 (1998).
[13] H. Sjöström, L. Hultman, J.-E. Sundgren, S. V. Hainsworth, T. F. Page, and G. S. A. M. Thenissen, J. Vac. Sci. Technol. A **14**, 56 (1996).
[14] N. Hellgren, M. P. Johansson, E. Broitman, L. Hultman, and J.-E. Sundgren, Phys. Rev. B **59**, 5162 (1999).
[15] G. A. J. Amaratunga, M. Chhowalla, C. J. Kiely, I. Alexandrou, R. Aharonov, and R. M. Devenish, Nature (London) **383**, 321 (1996).
[16] B. F. Coll, J. Jaskie, J. Markham, E. Menu, and A. Talin, *Amorphous Carbon State of the Art*, edited by S. R. P. Silva *et al.* (World Scientific, Singapore, 1998).
[17] B. Kleinsorge, A. C. Ferrari, J. Robertson, W. I. Milne, S. Waidmann, and S. Hearne, Diamond Relat. Mater. **9**, 643 (2000).
[18] M. Chhowalla, J. Robertson, C. W. Chen, S. R. P. Silva, C. A. Davis, G. A. J. Amaratunga, and W. I. Milne, J. Appl. Phys. **81**, 139 (1997).
[19] Y. Lifshitz, Diamond Relat. Mater. **8**, 1659 (1996).
[20] T. A. Friedmann, J. P. Sullivan, J. A. Knapp, D. R. Tallant, D. M. Follstaedt, D. L. Medlin, and P. B. Mirkarimi, Appl. Phys. Lett. **71**, 3820 (1997).
[21] V. I. Merkulov, D. H. Lowndes, G. E. Jellison, A. A. Puretzky, and D. B. Geohegan, Appl. Phys. Lett. **73**, 2591 (1998).
[22] J. Koskinen, J.-P. Hirvonen, and J. Keränen, J. Appl. Phys. **84**, 648 (1998).
[23] S. Sattel, J. Robertson, and H. Ehrhardt, J. Appl. Phys. **82**, 1 (1997).
[24] P. J. Fallon, V. S. Veeresamy, C. A. Davis, J. Robertson, G. A. J. Amaratunga, W. I. Milne, and J. Koskinen, Phys. Rev. B **48**, 4777 (1993).
[25] J. Fink, Adv. Electron. Electron Phys. **75**, 121 (1989).
[26] S. D. Berger, D. R. McKenzie, and P. J. Martin, Philos. Mag. Lett. **57**, 285 (1988).
[27] S. Prawer, K. W. Nugent, Y. Lifshitz, G. D. Lempert, E. Grossman, J. Kulik, I. Avigal, and R. Kalish, Diamond Relat. Mater. **5**, 433 (1996), Breit-Wigner-Fano function: $I(\omega)=I_0(\omega)(1+2(\omega-\omega_0)/q\Gamma)^2/[1+2(\omega-\omega_0)/\Gamma]^2$.
[28] F. Tuinstra and J. L. Koening, J. Chem. Phys. **53**, 1126 (1970).
[29] C. Mapelli, C. Castiglioni, C. Zerbi, and K. Mullen, Phys. Rev. B **60**, 12710 (1999).
[30] A. C. Ferrari and J. Robertson, Phys. Rev. B. (to be published).
[31] *Vacuum Arcs—Theory and Application*, edited by J. M. Lafferty (Wiley, New York, 1980).
[32] M. M. M. Bilek, M. Chhowalla, and W. I. Milne, Appl. Phys. Lett. **71**, 1777 (1997).
[33] Y. Lifshitz, S. R. Kasi, and J. W. Rabalais, Phys. Rev. Lett. **62**, 1290 (1989).
[34] R. Hytry, W. Möller, R. Wilhelm, and A. v. Keudell, J. Vac. Sci. Technol. A **11**, 2508 (1993).
[35] M. A. Elliott, P. W. May, J. Petherbridge, S. M. Leeds, M. N. R. Ashfold, and W. N. Wang, Diamond Relat. Mater. **9**, 311 (2000).
[36] M. Chhowalla, I. Alexandrou, C. Kiely, G. A. J. Amaratunga, R. Aharonov, and R. F. Fontana, Thin Solid Films **291**, 103 (1996).
[37] A. Stanishevsky, L. Khriachtchev, and I. Akula, Diamond Relat. Mater. **7**, 1190 (1998).
[38] J. Hartman, P. Siemroth, B. Schultrich, and B. Rauschenbach, J. Vac. Sci. Technol. A **15**, 2983 (1997); X. Shi, H. Fu, J. R. Shi, L. K. Cheah, B. K. Tay, and P. Hui, J. Phys.: Condens. Matter **10**, 9293 (1998).
[39] S. Waidmann, TU Dresden (personal communication); S. Waidmann, M. Knupfer, J. Fink, B. Kleinsorge, and J. Robertson, Diamond Related Mater. **9**, 722 (2000).
[40] R. A. Street, *Hydrogenated Amorphous Silicon* (Cambridge University Press, Cambridge, 1991).
[41] M. M. M. Bilek, P. J. Martin, and D. R. McKenzie, J. Appl. Phys. **83**, 2965 (1998).
[42] R. K. Dwivedi and R. K. Thareja, Phys. Rev. B **51**, 7160 (1995).
[43] Y. Yamagata, A. Sharma, J. Narayan, R. M. Mayo, J. W. Newman, and K. Ebihara, J. Appl. Phys. **86**, 4154 (1999).
[44] S. Grigull, W. Jacob, D. Henke, C. Spaeth, L. Sümmchen, and W. Sigle, J. Appl. Phys. **83**, 5185 (1998).
[45] M. Y. Chen and P. T. Murray, J. Vac. Sci. Technol. A **16**, 2093 (1998).
[46] N. Morrison, S. E. Rodil, J. Robertson, and W. I. Milne, 10th European Conference on Diamond, Diamond-like Materials, Carbon Nanotubes, Nitrides, and Silicon, Prague, September, 1999.
[47] M. Sakaki and T. Sakakibara, IEEE Trans. Plasma Sci. **22**, 1049 (1994).
[48] A. C. Ferrari, B. Kleinsorge, N. A. Morrison, A. Hart, V. Stolojan, and J. Robertson, J. Appl. Phys. **85**, 7191 (1999).
[49] M. Chhowalla, A. C. Ferrari, J. Robertson, and G. A. J. Amaratunga, Appl. Phys. Lett. **76**, 1419 (2000).
[50] G. A. J. Amaratunga, D. E. Segal, and D. R. McKenzie, Appl. Phys. Lett. **59**, 69 (1991).
[51] D. R. McKenzie, Y. Yin, N. A. Marks, C. A. Davis, B. A. Pailthorpe, G. A. J. Amaratunga, and V. S. Veeresamy, Diamond Relat. Mater. **3**, 353 (1994).
[52] F. J. Clough, W. I. Milne, B. Kleinsorge, J. Robertson, G. A. J. Amaratunga, and B. N. Roy, Electron. Lett. **32**, 498 (1996).
[53] C. Arena, B. Kleinsorge, J. Robertson, W. I. Milne, and M. E. Welland, J. Appl. Phys. **85**, 1609 (1999).